JMEPEG (2012) 21:2438–2445
DOI: 10.1007/s11665-012-0181-8

1059-9495/$19.00

In Situ Synthesis, Microstructure, and Properties of TiC and (Ti,W)C-Reinforced Fe-Mn-Al Austenitic Steel Matrix Composites

Ashok Kumar Srivastava and Karabi Das

(Submitted September 22, 2011; in revised form February 1, 2012)

In situ synthesis, microstructures, and properties of 10 vol.% TiC and (Ti,W)C-reinforced Fe-Mn-Al austenitic steel matrix composites have been reported in this paper. The microstructure of the prepared samples has been characterized by using scanning electron microscopy and X-ray diffraction technique. The abrasion wear resistance and mechanical properties such as hardness and impact energy of both the composites as well as the unreinforced Fe-Mn-Al austenitic steel have been evaluated. The (Ti,W)C-reinforced composite has higher impact energy and slightly lower hardness values compared to that of TiC-reinforced composite. The TiC-reinforced composite exhibits the best abrasive wear resistance of all the materials tested.

Keywords alloys, carbides, composites, microstructure, mechanical properties

1. Introduction

Metal matrix composites (MMCs) are a material which consists of metal alloys reinforced with particulates. MMCs produce a material whose mechanical properties are an intermediate between matrix alloy and ceramic reinforcement (Ref 1). A uniform distribution of reinforcing materials in the metal matrix offers improvement in strength, elastic modulus, corrosion, and wear resistance of resultant composites. Due to these properties, a particulate reinforced composite finds a wide range of applications in automotive and aerospace industries compared to their counterpart monolithic alloys (Ref 1). A large number of composite materials have metallic matrices reinforced with high strength, high modulus, and often brittle ceramic phase particles (Ref 2). There are several reviews available on processing, properties, and interfacial phenomenon in composites (Ref 3-6). Iron-based alloys or steels have been used frequently as matrix materials for MMCs owing to their low cost, versatility, and adequate mechanical properties. The addition of hard ceramic particles into steel matrices provides a more practical way of increasing the hardness of steels.

Pagounis and coworkers reported that the wear resistance of steels can be improved dramatically by the incorporation of ceramic particles such as carbides and oxides (Ref 7). The most common ceramic materials used for reinforcing of various types of steel matrices are Al_2O_3, ZrO_2, Si_3N_4, Cr_3C_2, TiN, TiB_2, TiC, B_4C, WC, VC, etc. (Ref 7, 8). Titanium carbide (TiC) is one of the most useful ceramics in modern engineering applications because of its high hardness, high wear resistance, high melting point, good chemical inertness, high Young's modulus, and thermal conductivity as well as high thermal shock resistance and its incorporation can be expected to improve the abrasion resistance of many different alloy systems (Ref 9). The fabrication of MMCs using the solidification and casting technique is particularly attractive owing to low viscosity of liquid metals which permits low cost, net-shape fabrication, adaptability of casting processes to existing production practices, and flexibility in designing the structure through controlled solidification.

In the present investigation, the Fe-Mn-Al austenitic steel is chosen as the matrix and the TiC and (Ti,W)C are chosen as the reinforcements. The (Ti,W)C as reinforcements in steel and iron alloy melts may be more appropriate because its density (6.66 g/cm^3 for ($Ti_{0.75}W_{0.25}$)C (Ref 10) and 9.1 g/cm^3 for ($Ti_{0.5}W_{0.5}$)C (Ref 11)) is higher than that of TiC (4.25 g/cm^3) and close to that of iron melt (7.8 g/cm^3) resulting in less segregation. The hardness of (Ti_{1-x},W_x)C (19-21 GPa (Ref 12)) is more or less the same as that of TiC (18-23 GPa (Ref 13)). However, the fracture toughness of (Ti_{1-x},W_x)C (6.4-7.7 MPa $m^{1/2}$ (Ref 12)) is higher than that of TiC (3.5-4.3 MPa $m^{1/2}$ (Ref 13)) and this may result in better mechanical properties of the (Ti_{1-x},W_x)C-reinforced composite compared to those of the TiC-reinforced composite.

The present work highlights the microstructural characterization, mechanical properties such as hardness and impact energy, and abrasive wear resistance of the TiC and (Ti,W)C-reinforced Fe-Mn-Al austenitic steel matrix composites.

2. Experimental Procedure

The main raw materials used to produce the composites are listed in Table 1. Apart from these raw materials, Al, Cr, and

Ashok Kumar Srivastava, Department of Metallurgical Engineering, O. P. Jindal Institute of Technology, Punjipathra, Raigarh 496001, Chhattisgarh, India; and **Karabi Das**, Department of Metallurgical and Materials Engineering, Indian Institute of Technology, Kharagpur, Kharagpur 721302, West Bengal, India. Contact e-mail: ashok.iitkgp@yahoo.co.uk.

Fe-Si alloy were also used to adjust the compositions of the composites. All raw materials were exactly weighed to achieve the nominal compositions of 10 vol.% TiC and (Ti,W)C-reinforced Fe-Mn-Al austenitic steel matrix composites. The synthesis of the composites was carried out in a 25 kg high frequency induction furnace (Inductotherm, India) in air, where the melt was covered with a ceramic block to prevent the oxidation of the melt to a certain extent. The steel scrap and cast iron were initially heated to 1600 °C and maintained at this temperature for 15 min and then the temperature was raised to 1625 °C. The calculated amount of ferro-titanium (70% purity) and electrolytic manganese (95% purity), and ferro-tungsten (74% purity) and electrolytic manganese were added to the melt by the plunging method at 1625 °C for TiC and (Ti,W)C-reinforced composite materials, respectively. The melt was stirred continuously at this temperature for 10 min with an iron rod, which was inserted into the melt through a small hole located at the center of the ceramic covering block followed by pouring in a metallic mould. The nominal compositions of the unreinforced matrix alloy as well as the composite materials are presented in Table 2.

Samples of dimension 12 mm × 12 mm × 10 mm for scanning electron microscopy (SEM) were cut from the middle portion of the cast material. Then, the samples were polished using conventional polishing techniques and etched with 2% nital (2 mL HNO_3 + 98 mL ethanol). The microstructure was characterized by SEM (JEOL, JSM-5800) equipped with an energy-dispersive X-ray analyzer (EDS). Phase identification of the composites was performed by X-ray diffraction (XRD) (PW-1710) analysis with Co K_α radiation.

The hardness was measured using Vickers hardness tester at an applied load of 30 kgf and loading time of 20 s. The samples were first surface finished and at least ten measurements were taken randomly in each sample and averaged to obtain the hardness of the specimen. Microhardness of the matrix and individual phases were measured using Vickers microhardness tester (Model Leica VMHT) under a load of 50 gf and a dwell time of 20 s at room temperature. The charpy impact energy testing was carried out at room temperature in accordance with ASTME23-88 standard V-notch specimen having 10 × 10 mm^2 cross section and 55 mm length. A 45° 'V' notch having 0.25 mm notch root radius and 2 mm notch depth was made at the mid point along the length of the sample. The average of three measurements has been taken as the impact energy of the materials.

Dry-sliding abrasive wear tests were carried out using a computer aided pin-on-disc wear-testing machine (TR-201 M4, DUCOM, Bangalore, India) in air at room temperature at the normal loads of 50 and 100 N. Wear tests were conducted in dry conditions to avoid the effect of lubricating medium. In this method, the test specimens were clamped in the holder and held by a load applied by a lever mechanism against the surface of a 220 grit SiC abrasive paper stuck to a grinding disc, which rotated at 500 rev min^{-1}. A fixed track diameter of 40 mm was used in all the tests. All the tests were run for a total distance of 2 km at a constant sliding speed of 1 m s^{-1}. The tangential force due to friction was measured during sliding. During wear testing, two plots, i.e., height loss (μm) versus time (s) and force of friction (F) versus time (s) were generated. The sliding distance is calculated by multiplying the time with sliding velocity (V = 1 m s^{-1}) and volume loss (mm^3) is calculated by multiplying the height loss (μm) with the area of cross section (mm^2). The wear rate is defined as the ratio of wear volume to the sliding distance. The computer aided pin-on-disc wear-testing machine used in the present study gives the force of friction (F) directly as one of the outputs. The coefficient of friction (μ) is taken as the ratio of the force of friction (F) and the normal load (N) applied.

Table 1 The nominal compositions (wt.%) of the main raw materials

Raw materials	C	Mn	Si	Al	Cr	S	P
Steel scrap	0.049	0.43	0.028	0.003	0.035	0.013	0.023
Cast iron	4.5	0.043	1.05	…	…	0.043	0.175

3. Results and Discussion

3.1 Microstructural Study

The SEM micrograph (Fig. 1a) of TiC-reinforced composite reveals that the microstructure consists of three phases: the austenite matrix, discrete ferrite, and TiC particle. The EDX spectrum (Fig. 1b) taken from the TiC particle confirms the formation of TiC in the matrix. XRD pattern (Fig. 2) of the composite confirms the formation of austenite, ferrite, and TiC phases.

Figure 3(a) and (b) shows the SEM micrographs of (Ti,W)C-reinforced composite at low and high magnification, respectively. SEM examination of the microstructure shows that (Ti,W)C has the same kind of typical morphology as that of TiC. The microstructure consists of austenite, ferrite, and (Ti,W)C phases, which has been confirmed with the existing peaks of XRD pattern of (Ti,W)C-reinforced composite, as shown in Fig. 4. The EDX spectra taken from the center and periphery of (Ti,W)C particle show that the amount of W is more at the periphery compared to the same at the center (Fig. 3c and d). The values of W/Ti ratio reveals that the concentration of titanium decreases whereas the concentration of tungsten increases from the core to periphery of the (Ti,W)C particles (Table 3). The mechanism for the formation of (Ti,W)C particles in the composites has been discussed elsewhere (Ref 14).

3.2 Mechanical Properties

3.2.1 Hardness. It has been observed from Fig. 5 that the hardness of the composites is significantly higher than that of the unreinforced matrix alloy, which is due to the presence of

Table 2 Chemical compositions (wt.%) of unreinforced and reinforced Fe-Mn-Al austenitic steel

Materials	C	Mn	Si	Al	Cr	S	P	Ti	W
Fe-Mn-Al austenitic steel	1.09	16.94	0.36	3.25	0.46	0.013	0.087	…	…
TiC-reinforced composite	1.38	17.20	0.40	3.42	0.44	0.024	0.080	10.00	…
(Ti,W)C-reinforced composite	1.40	17.25	0.38	3.30	0.38	0.021	0.081	3.0	3.05

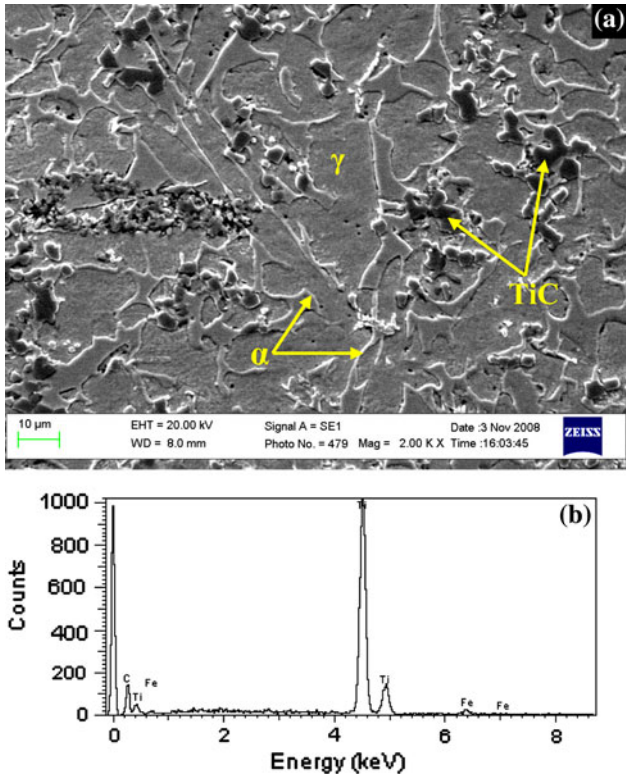

Fig. 1 (a) SEM micrograph of TiC-reinforced composite and (b) EDX spectra from TiC

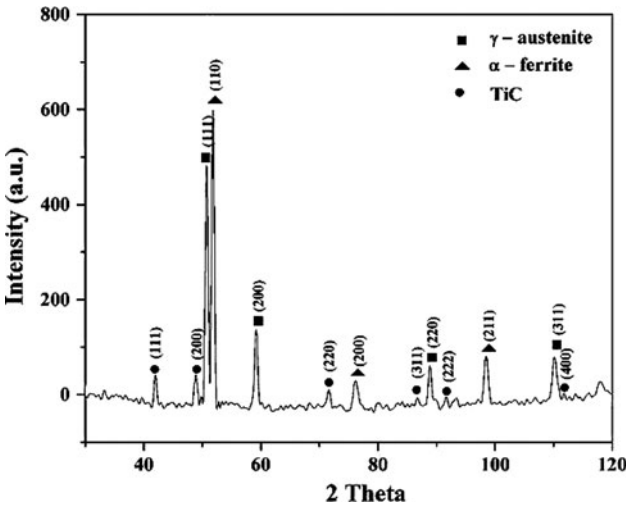

Fig. 2 XRD pattern of TiC-reinforced composite

hard TiC and (Ti,W)C reinforcing particles in the composites. The hardness of TiC-reinforced composite is higher than that of (Ti,W)C-reinforced composite. The hardness of a composite material depends on the size, volume fraction, and hardness of the reinforcement. It also depends on the hardness of the matrix.

The size and measured microhardness values of (Ti,W)C (22-26 GPa) and TiC (21-27 GPa) are same. The targeted volume fraction of TiC and (Ti,W)C was 10%. However, image analysis shows that although the volume fraction of TiC is ~10%, the volume fraction of (Ti,W)C is ~9%. A higher

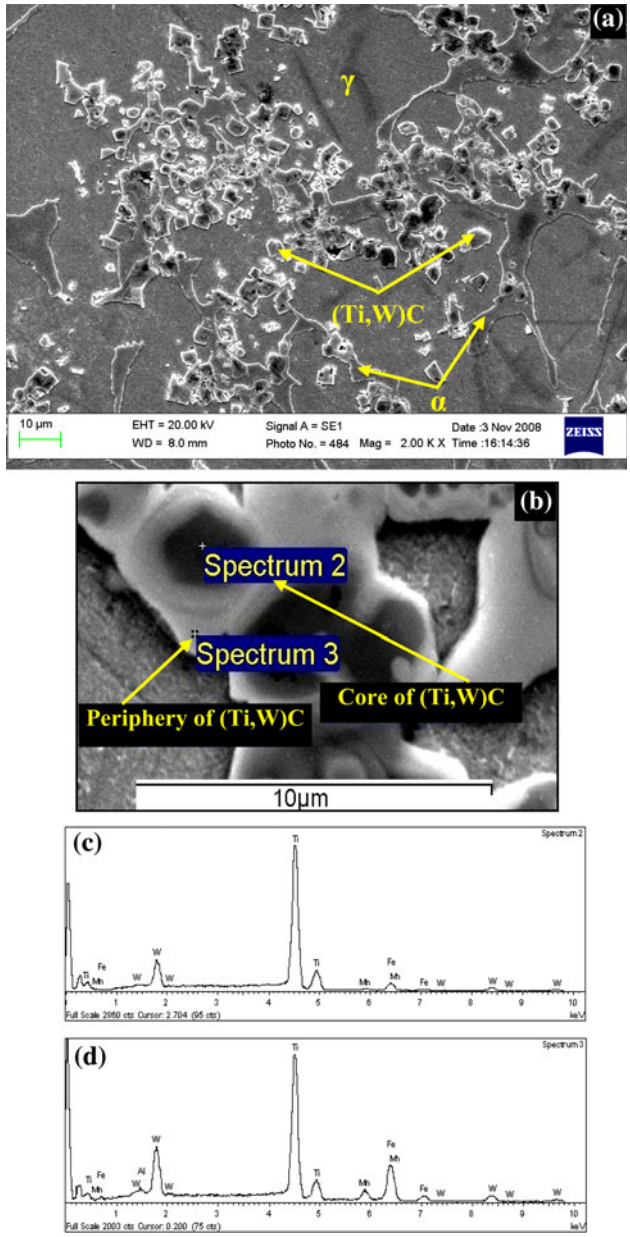

Fig. 3 SEM micrographs of (Ti,W)C-reinforced composite at (a) low and (b) high magnification and EDX spectrum of (c) core and (d) periphery of (Ti,W)C particle

volume fraction of TiC compared to (Ti,W)C is a contributing factor towards the increased hardness of TiC-reinforced composite over (Ti,W)C-reinforced composite. The matrix compositions of both the composites are same. However, the matrix microhardness of TiC and (Ti,W)C-reinforced composite are 390 and 360 HV, respectively. A higher volume fraction of TiC particles in TiC-reinforced composite develops more particle-matrix area. Higher the amount of particle-matrix interface area, more is the hardening due to dislocations resulting higher matrix microhardness of TiC-reinforced composite. The coefficient of thermal expansions (CTEs) mismatch between the matrix and reinforcement also plays a role in the hardening behavior of the matrix. The CTE of TiC, (Ti,W)C, and the matrix are 5.5×10^{-6}, 7.3×10^{-6}, and $1.7\text{-}2.5 \times 10^{-5}$/°C, respectively. The CTE mismatch between the reinforcement and matrix is more in (Ti,W)C-reinforced composite compared

to the same in TiC-reinforced composite. Hence, the amount of residual plastic strain in the matrix around the particle is more in (Ti,W)C-reinforced composite resulting higher matrix hardness. Therefore, it appears that the effect of interfacial area is more predominant than the effect of CTE mismatch resulting higher matrix hardness of TiC-reinforced composite than that of (Ti,W)C-reinforced composites.

3.2.2 Impact Energy. A large drop in the impact energy values (Fig. 5) after the addition of TiC and (Ti,W)C particles in Fe-Mn-Al austenitic steel can be attributed to the brittle nature of the reinforcing carbide particles which reduces the deformation capability of the composites. A slightly higher impact toughness of (Ti,W)C-reinforced composite compared to TiC-reinforced composite can be attributed to the formation of strong interface between the (Ti,W)C reinforcing particles and matrix. It has been reported in the literature that the formation of strong interface between the reinforcing particles and matrix results in an increase in the impact toughness of the composite (Ref 15). Diffusion of W atom in the TiC particles by substituting Ti atoms make the interface between the matrix and (Ti,W)C particles stronger than that of the same between the matrix and TiC particles. The formation mechanism of TiC and (Ti,W)C reinforcing particles in the matrix has been discussed in detail in another paper (Ref 14). The higher fracture toughness of (Ti,W)C particles compared to TiC particles can

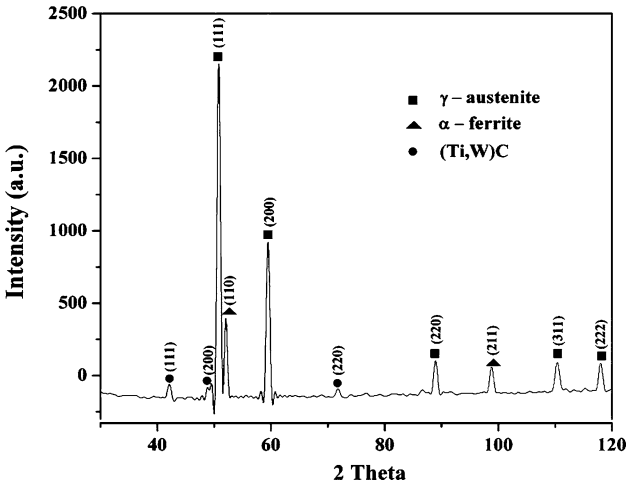

Fig. 4 XRD pattern of (Ti,W)C-reinforced composite

Table 3 W/Ti ratio of core and periphery in (Ti,W)C-reinforced composite

Spectrum	Ti	W	W/Ti
Core	72.61	18.83	0.259
Periphery	47.35	24.20	0.511

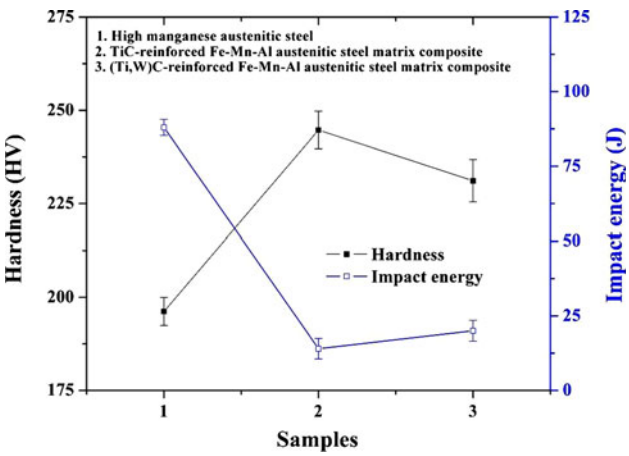

Fig. 5 Hardness and impact energy values of Fe-Mn-Al austenitic steel, and TiC and (Ti,W)C-reinforced composites

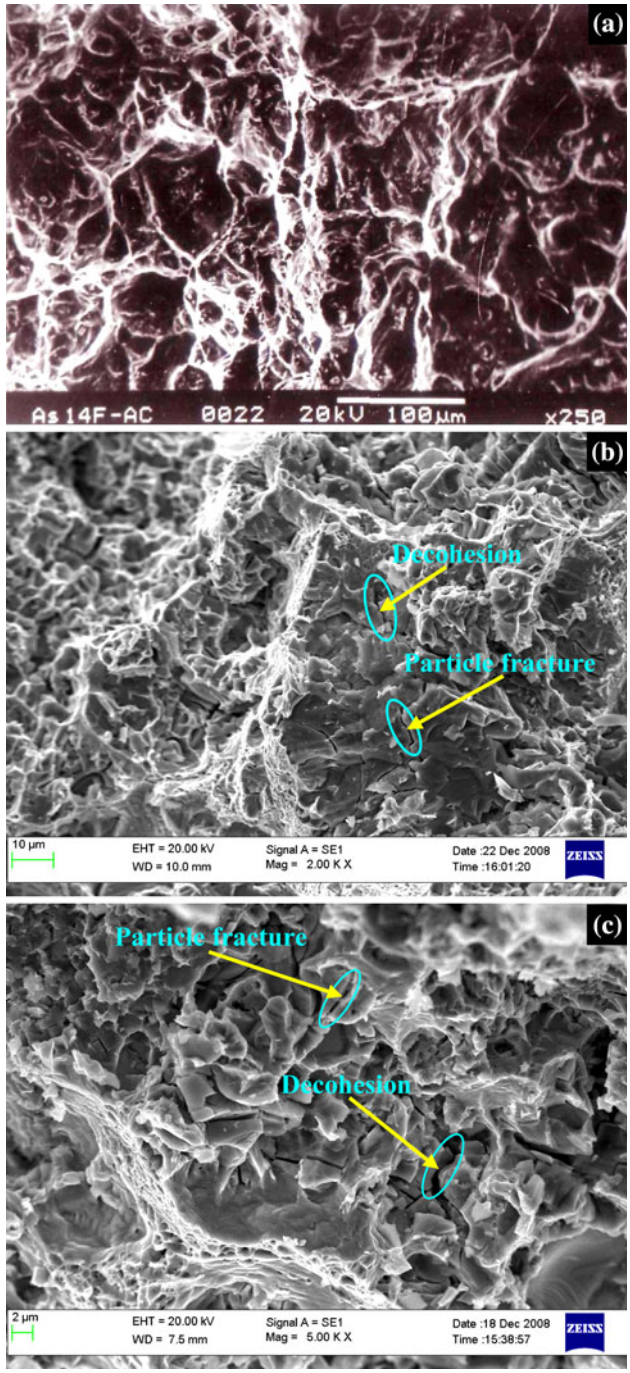

Fig. 6 SEM micrographs of the fractured surfaces of (a) Fe-Mn-Al austenitic steel, and (b) TiC and (c) (Ti,W)C-reinforced composites

be the other contributing factor to increase the impact toughness of (Ti,W)C-reinforced composite compared to TiC-reinforced composite.

Figure 6(a)-(c) shows the SEM micrographs of the fractured surfaces of Fe-Mn-Al austenitic steel, and TiC and (Ti,W)C-reinforced composites, respectively. A typical ductile fracture with large number of dimples has been revealed in the fractograph (Fig. 6a) of Fe-Mn-Al austenitic steel. The fractographs (Fig. 6b and c) of TiC and (Ti,W)C-reinforced composites show quasi-cleavage type fracture with some scattered dimples. It has been observed from the fractographs of the composites that there are two basic modes of fracture occur, namely: the interfacial decohesion and particle fracture. It has been reported in the literature that the mode of fracture depends on the relative strength of the interface and matrix (Ref 16). When load is applied, the matrix plastically deforms and then transforms the stress to the particles. The fracture of the particles occurs as soon as the threshold stresses is reached and decohesion occurs when the average stress in the particles surpassed a critical value known as the interface strength. It has been already mentioned that the (Ti,W)C particles have higher fracture toughness than that of the TiC particles. The (Ti,W)C particles also form a stronger interface with the matrix compared to the same in TiC-reinforced composite. Hence, the (Ti,W)C particles with higher fracture toughness and better bonding with the matrix are often barrier to the reinforcement damage and decohesion, respectively. Thus the (Ti,W)C-reinforced composite is more ductile than that of the TiC-reinforced composite.

3.3 Abrasive Wear Resistance

Figure 7(a) and (b) shows the variation of volume loss and wear rate of the composites and unreinforced matrix alloy with sliding distance under the loads of 50 and 100 N, respectively. It can be seen that the volume loss and wear rate of the composites is lower than that of the unreinforced Fe-Mn-Al austenitic steel. The abrasive wear resistance is defined as the inverse of volume loss (Ref 17). The increase of the abrasive wear resistance of the composites compared to unreinforced matrix alloy can be attributable to the higher hardness of the

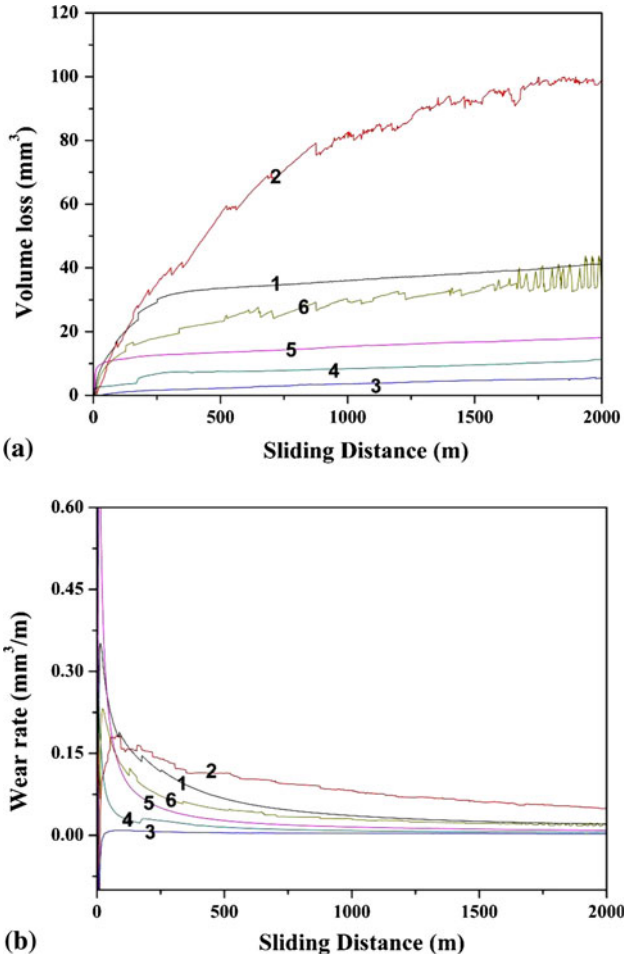

Fig. 7 (a) Volume loss and (b) wear rate versus sliding distance of Fe-Mn-Al austenitic steel at 50 and 100 N (1 and 2), TiC-reinforced composite at 50 and 100 N (3 and 4) and (Ti,W)C-reinforced composite at 50 and 100 N (5 and 6)

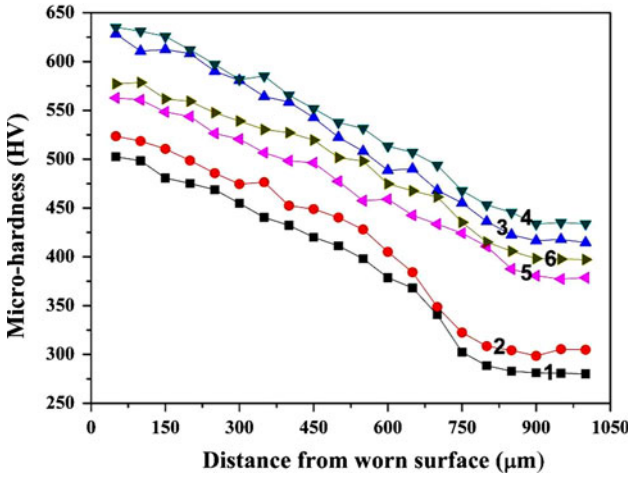

Fig. 8 Variation of the matrix microhardness with distance from the top worn surface of Fe-Mn-Al austenitic steel at 50 and 100 N (1 and 2), TiC-reinforced composite at 50 and 100 N (3 and 4) and (Ti,W)C-reinforced composite at 50 and 100 N (5 and 6)

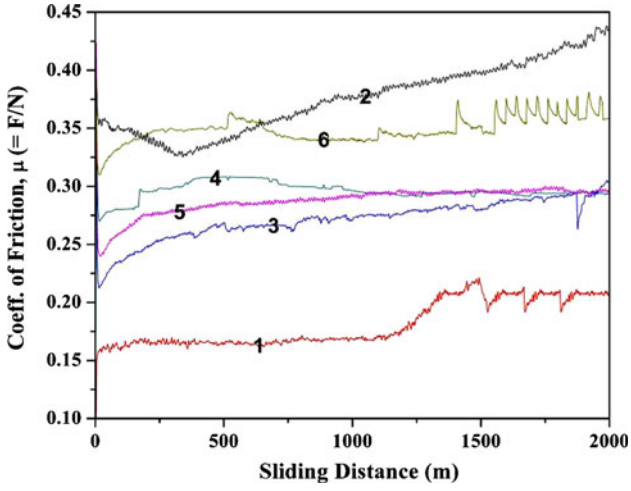

Fig. 9 Coefficient of friction (μ) versus sliding distance of Fe-Mn-Al austenitic steel at 50 and 100 N (1 and 2), TiC-reinforced composite at 50 and 100 N (3 and 4) and (Ti,W)C-reinforced composite at 50 and 100 N (5 and 6)

composites due to the incorporation of TiC and (Ti,W)C particles and decrease of the contact area between the matrix of the composite and abrasive particle due to the presence of TiC and (Ti,W)C particles. The TiC and (Ti,W)C particles also act as load carrying elements and inhibitors against plastic deformation of matrix. The higher volume loss and wear rate of (Ti,W)C-reinforced composite compared to TiC-reinforced composite can be attributed to the higher hardness of TiC-reinforced composite compared to (Ti,W)C-reinforced composite. The effect of load in increasing the volume loss and wear rate is more pronounced in unreinforced matrix alloy compared to the composites. However, at both loads, abrasive wear resistance of the composites is better than that of the unreinforced matrix alloy. In the case of unreinforced matrix alloy, grits plough more deeply into the surface as the load increases, while in composites the hard TiC and (Ti,W)C particles act as barrier to the penetration of the grits (abrasive particles) and protect the softer matrix. The plots of volume loss and wear rate versus sliding distance exhibit some fluctuation in the curve. This is possibly due to the trap and release of the debris particles in between the sliding surfaces.

Figure 8 shows the variation of matrix microhardness with distance from the top worn surface along the cross section of the specimens. It can be seen that the surface layers are much harder than the inner core of the specimens. The increase in surface hardness can only be possible through work hardening accompanying the plastic deformation of surface layers. A plastic strain which is induced in the subsurface region of ductile matrix during sliding wear test generally increases with applied load (Ref 18), which is obvious from Fig. 8 that the hardness of surface layer increases with increasing the applied load.

The variations in the coefficient of friction versus sliding distance (Fig. 9) curve reveal the formation of wear debris on the sliding surface. The plot shows the constancy of the coefficient of friction when the constant amount of debris is

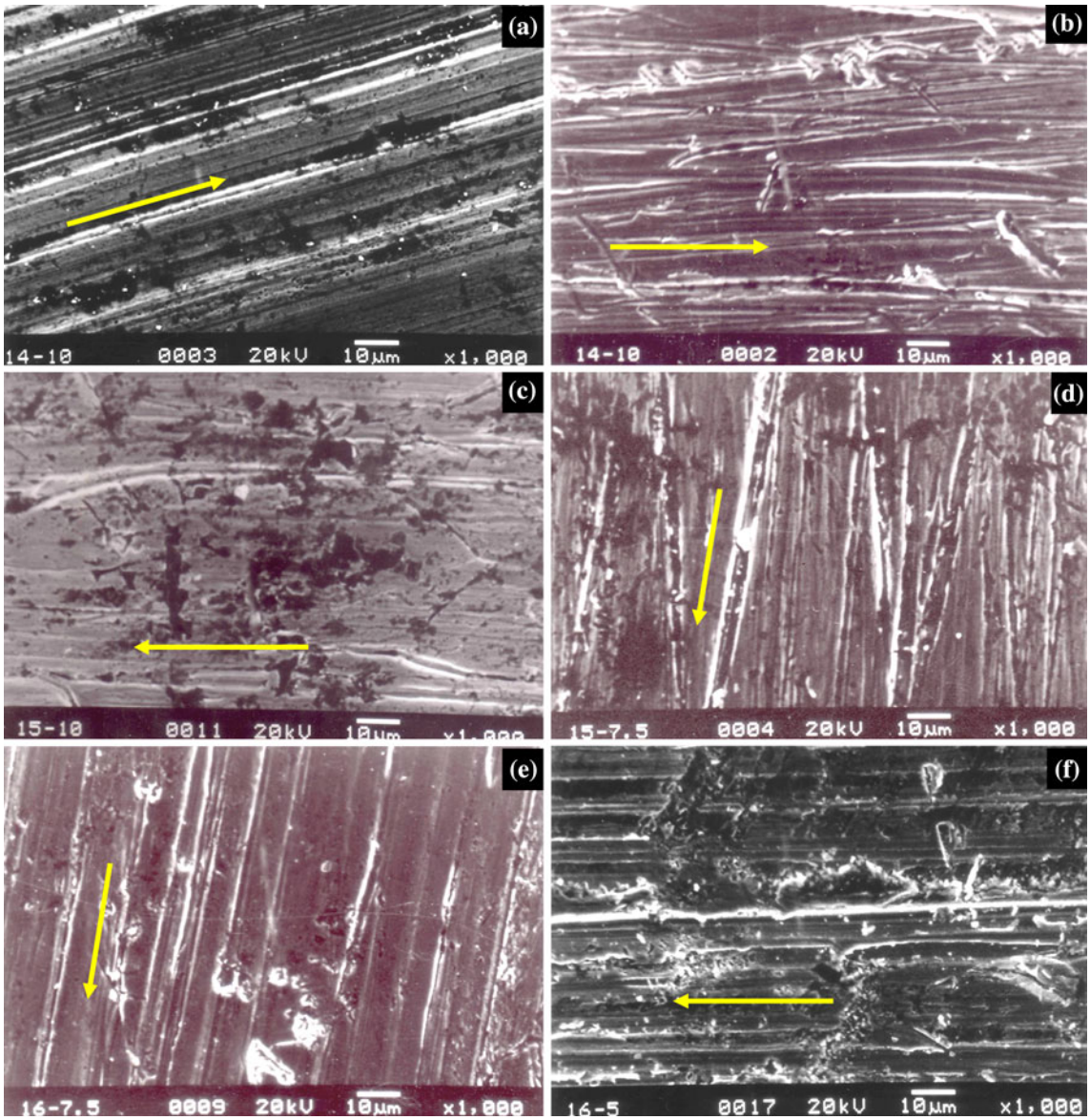

Fig. 10 SEM micrographs of the worn surface of (a and b) Fe-Mn-Al austenitic steel, (c and d) TiC and (e and f) (Ti,W)C-reinforced composites at the load of 50 and 100 N

present on the sliding surface while the increase and decrease in the coefficient of friction states the build up and elimination of wear debris on the sliding surface, respectively. It can be seen from Fig. 9 that the coefficient of friction of unreinforced and reinforced Fe-Mn-Al austenitic steel increases with increasing the applied normal load. The roughness of true contact surface between the wear specimen and abrasive paper during sliding wear increases with increasing the applied load. It has been reported in the literature that the friction gets higher with increasing roughness of the surface (Ref 19). Therefore, the coefficient of friction increases with the applied loads. It can be seen that as the load increases the increase of the coefficient of friction of the unreinforced matrix alloy is higher than that of the composites, which might be due to the resisting nature of TiC and (Ti,W)C particles towards material removal resulting in lower increase rate of the coefficient of friction of the TiC and (Ti,W)C-reinforced composites.

The SEM micrographs of the worn surfaces of unreinforced and reinforced Fe-Mn-Al austenitic steel tested at the loads of 50 and 100 N are shown in Fig. 10a-f. In all the SEM micrographs, an arrow mark is shown to indicate the sliding direction. The worn surfaces (Fig. 10a and b) of Fe-Mn-Al austenitic steel show that the soft matrix has been cut by hard abrasive SiC particles, leaving traces of deformation in the form of microploughing and grooving. The material of the specimen is displaced to both sides of wear grooves as the ductile surface is abraded by the hard abrasive SiC particles. The SEM micrographs (Fig. 10c and d) of the worn surface of TiC-reinforced composite show that the surface appears much rougher. Similar morphology of the worn surface of (Ti,W)C-reinforced composite (Fig. 10e and f) has been observed. The abrasive SiC particles cut the ductile matrix of the TiC and (Ti,W)C-reinforced composites during the early stages of abrasive wear test. They remove the material as chips from

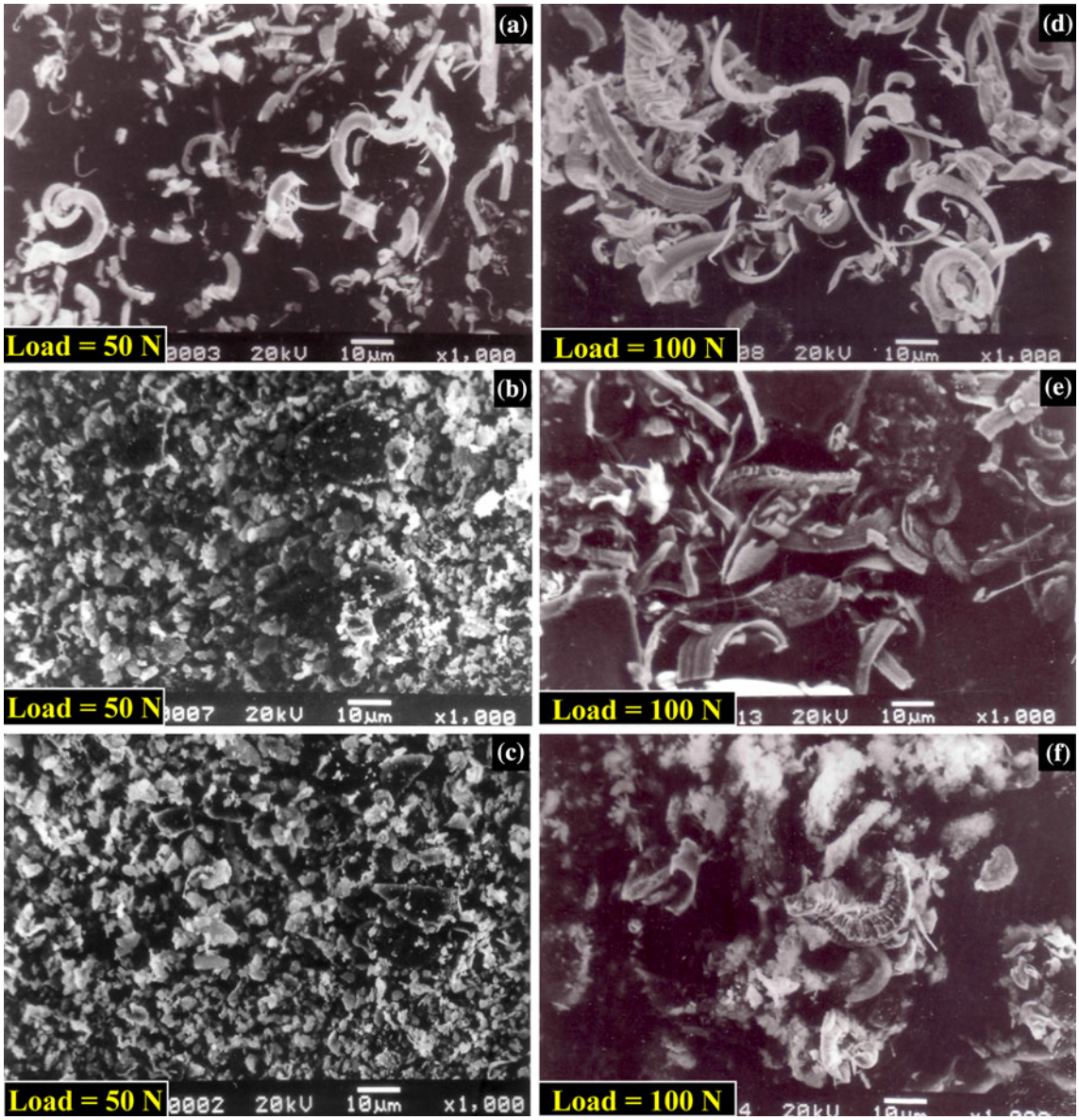

Fig. 11 SEM micrographs of the wear debris of (a and d) Fe-Mn-Al austenitic steel, (b and e) TiC and (c and f) (Ti,W)C-reinforced composites at the load of 50 and 100 N

the grooves of the surface. As a result, the TiC and (Ti,W)C reinforcing particles are protruded to the surface of the TiC and (Ti,W)C-reinforced composites, respectively. Thus the reinforcing particles are in direct contact with abrasive SiC particles. The interaction of the TiC and (Ti,W)C reinforcing particles with abrasive SiC particles lead to the fragmentation and blunting of the abrasive particles. Thus the severity of the microcutting action of the blunted abrasive particles is considerably reduced. Continuous wear results in repeated plastic deformation of the surface and fragmentation of the abrasive SiC particles, leading to the rough surfaces of the composites. It has been observed that the plastic ploughing is mild at low load (50 N), and more severe when the load is increased to 100 N in both the unreinforced and reinforced Fe-Mn-Al austenitic steel. The dark appearance of the worn surfaces can be contributed to the formation of oxide layers due to frictional heating which fills out the abrasive grooves.

A close examination of the nature of the wear debris of unreinforced matrix alloy reveals that at both 50 and 100 N loads, the wear debris comprises a mixture of particles and ribbon type metallic chips (Fig. 11a and d). However, in the case of the composites, it can be seen that at 50 N load, the wear debris is in the form of fine particles (Fig. 11b and c), and at the load of 100 N, the wear debris comprises a mixture of fine particles and ribbon type metallic chips (Fig. 11e and f). The formation of fine debris may be due to continuous rubbing action of samples on the wear track while ribbon type debris are the characteristics of cutting and ploughing action of hard abrasive particles.

4. Summary

A reasonably uniform distribution of the 10 vol.% TiC and (Ti,W)C-reinforcement phases in Fe-Mn-Al austenitic steel has been achieved using conventional melting and casting route. Based on the results, the impact toughness of (Ti,W)C-reinforced composite is higher than that of TiC-reinforced composite while the hardness and abrasive wear resistance of the same is lower compared to TiC-reinforced composite. Based on the present investigation, it can be concluded that the TiC and (Ti,W)C-reinforced composites have considerable potential for use in structural applications.

Acknowledgment

The authors wish to acknowledge Naval Research Board, New Delhi, India, for sponsoring this research work.

References

1. M.M. Schwartz, *Composite Materials. Vol II: Processing, Fabrication, and Applications*, Prentice Hall, Englewood Cliffs, NJ, 1996, p 1–276
2. D.J. Lloyd, Particle Reinforced Aluminium and Magnesium Matrix Composites, *Int. Mater. Rev.*, 1994, **39**, p 1–23
3. P.K. Rohatgi, R. Asthana, and S. Das, Solidification, Structures and Properties of Cast Metal-Ceramic Particle Composites, *Int. Met. Rev.*, 1986, **31**(3), p 115–139
4. R. Asthana and S.N. Tewari, Interfacial and Capillary Phenomena in Solidification Processing of Metal-Matrix Composites, *Compos. Manuf.*, 1993, **4**(1), p 3–25
5. T.S. Srivatsan, T.S. Sudarshan, and E.J. Lavernia, Processing of Discontinuously-Reinforced Metal-Matrix Composites by Rapid Solidification, *Prog. Mater. Sci.*, 1995, **39**(4–5), p 317–409
6. E.J. Lavernia and Y. Wu, *Spray Atomization and Deposition*, John Wiley and Sons Ltd., Chichester, 1996, p 383–474
7. E. Pagounis and V.K. Lindroos, Processing and Properties of Particulate Reinforced Steel Matrix Composites, *Mater. Sci. Eng. A*, 1998, **246**, p 221–234
8. K. Das, T.K. Bandyopadhyay, and S. Das, A Review on the Various Synthesis Routes of TiC Reinforced Ferrous Based Composites, *J. Mater. Sci.*, 2002, **37**, p 3881–3892
9. Ö.N. Doğan, J.A. Hawk, J.H. Tylczak, R.D. Wilson, and R.D. Govier, Wear of Titanium Carbide Reinforced Metal Matrix Composites, *Wear*, 1999, **225–229**, p 758–769
10. W.H. Jiang, J. Fei, and X.L. Han, In Situ Synthesis of (TiW)C/Fe Composites, *Mater. Lett.*, 2000, **46**, p 222–224
11. E.O. Correa, N.G. Alcantara, D.G. Tecco, and R.V. Kumar, Development of an Iron-Based Hardfacing Material Reinforced with Fe-(TiW)C Composite Powder, *Met. Mater. Trans. A*, 2007, **38**, p 937–945
12. J. Jung and S. Kang, Sintered (Ti, W)C Carbides, *Scripta Mater.*, 2007, **56**, p 561–564
13. W. Acchar and C.A. Cairo, The Influence of (Ti, W)C and NbC on the Mechanical Behavior of Alumina, *Mater. Res.*, 2006, **9**, p 171–174
14. A.K. Srivastava and K. Das, Microstructure and Abrasive Wear Study of (Ti, W)C-Reinforced High-Manganese Austenitic Steel Matrix Composite, *Mater. Lett.*, 2008, **62**, p 3947–3950
15. T. Ozben, E. Kilickap, and O. Çakır, Investigation of Mechanical and Machinability Properties of SiC Particle Reinforced Al-MMC, *J. Mater. Process. Technol.*, 2008, **198**, p 220–225
16. R. Hadian, M. Emamy, N. Varahram, and N. Nemati, The Effect of Li on the Tensile Properties of Cast Al-Mg_2Si Metal Matrix Composite, *Mater. Sci. Eng. A*, 2008, **490**, p 250–257
17. S.C. Tjong and K.C. Lau, Abrasion Resistance of Stainless-Steel Composites Reinforced with Hard TiB_2 Particles, *Compos. Sci. Technol.*, 2000, **60**, p 1141–1146
18. J. Zhang and A.T. Alpas, Wear Regimes and Transitions in $A1_2O_3$ Particulate-Reinforced Aluminium Alloys, *Mater. Sci. Eng. A*, 1993, **160**, p 25–35
19. M. Sedlaček, B. Podgornik, and J. Vižintin, Influence of Surface Preparation on Roughness Parameters, Friction and Wear, *Wear*, 2009, **266**, p 482–487